symmetry

MDPI

Article

Studies of Deformed Halo Structures of ^{39}Na and ^{42}Mg

Qingzhen Chai [1], Hongxing Chen [1], Minghao Zha [1], Junchen Pei [2,*] and Furong Xu [2]

[1] Department of Physics, Henan University of Technology, Zhengzhou 450001, China; chaiqz@haut.edu.cn (Q.C.); 201821020111@stu.haut.edu.cn (H.C.); icydonutlcp@gmail.com (M.Z.)
[2] State Key Laboratory of Nuclear Physics and Technology, School of Physics, Peking University, Beijing 100871, China; frxu@pku.edu.cn
* Correspondence: peij@pku.edu.cn

Abstract: Background: The recent experimental discovery of drip-line nucleus ^{39}Na has attracted great interest in theoretical studies of exotic nuclear structures in this mass region. **Methods:** We solve the Skyrme–Hartree–Fock–Bogoliubov (Skyrme-HFB) equation within deformed coordinate-spaces. The present approach is suitable for descriptions of weakly bound deformed nuclei with continuum effects and deformed halo structures. **Results:** The systematical two-neutron separation energies are obtained with the SkM$^*_{\rm ext1}$ and UNEDF0$_{\rm ext1}$ forces for Na and Mg isotopes close to the neutron drip line. The density distributions show that ^{39}Na and ^{42}Mg have deformed halo structures. Furthermore, there are significant influences of various pairing interactions on halo shapes at large distances. **Conclusions:** Both ^{39}Na and ^{42}Mg are very weakly bound with well prolate deformed cores. However, their surface halo structures are dependent on the choices of pairing interactions. The volume-type pairing interaction tends to predict a prolate deformed halo, while the halo deformations at large distances are reduced by adopting the surface pairing. We demonstrate that ^{39}Na and ^{42}Mg are promising candidates for two-neutron deformed halo nuclei.

Keywords: deformed halos; Hartree–Fock–Bogoliubov; pairing interaction

Citation: Chai, Q.; Chen, H.; Zha, M.; Pei, J.; Xu, F. Studies of Deformed Halo Structures of ^{39}Na and ^{42}Mg. *Symmetry* **2022**, *14*, 215. https://doi.org/10.3390/sym14020215

Academic Editors: Floyd W. Stecker and Ignatios Antoniadis

Received: 17 December 2021
Accepted: 20 January 2022
Published: 23 January 2022

1. Introduction

Exploring exotic nuclear structures far away from the β-decay stable line is one of the major scientific goals in rare-isotope beam facilities around the world. Of particular interest is the halo structure, which is characterized by significant extensions of neutron or proton density distributions at nuclear surfaces [1–6]. There were extensive experimental studies to look for halo structures [7]. Some one-neutron and two-neutron halos have been discovered by experiments, which have attracted strong theoretical interests. However, deformed halo structures are rare, and two-neutron deformed halos are still absent in nature.

Recently, the drip-line nuclei ^{31}F and ^{34}Ne have been reconfirmed by experiments in RIKEN [8]. In this experiment, one event of ^{39}Na was also observed. ^{39}Na is mostly likely to be the drip line of sodium isotopes and is a promising two-neutron halo nucleus. Besides, the neighboring ^{40}Mg has been observed [9] and the drip line of magnesium is still not known. Both ^{39}Na and ^{40}Mg have a magic neutron number $N = 28$, but this neuron shell is broken near the neutron drip line [10]. Previous theoretical studies have consistently predicted that ^{40}Mg is a prolate deformed nuclei [10–12]. In deformed weakly bound nuclei, the interplay between continuum, pairing correlations, halo structures and deformations is particularly intriguing.

The suitable microscopic tool for descriptions of weakly bound deformed nuclei in the framework of nuclear density functional theory is the coordinate-space formulation of the Hartree–Fock–Bogoliubov (HFB) method [13,14]. The ab initio methods can also describe weakly bound spherical nuclei, but this is difficult for deformed shapes. The coordinate-space HFB can discretize the quasiparticle continuum and resonances rather precisely and is able to describe deformed halo asymptotics within large boxes. In HFB calculations,

Skyrme forces [15] are commonly adopted as non-relativistic effective nucleon–nucleon interactions. There are many Skyrme parameterizations developed with different physics purposes. For example, SkM* forces [16] are widely used in fission studies for reasonable descriptions of fission barriers. SLy4 force [17] has good isotopic properties towards drip lines and is widely used in descriptions of neutron stars. UNEDF0 force [18] has a very small rms of 1.455 MeV regarding global binding energies. Furthermore, extended Skyrme forces with additional higher-order density dependent terms are expected to improve the global theoretical descriptions [19,20]. Generally, different effective interactions can lead to very different drip-line locations although they all are good at descriptions of stable nuclei.

In the present work, we aim to study deformed halo structures of ^{39}Na and ^{42}Mg. The calculations are performed based on the self-consistent Skyrme-HFB approach in a large, axially symmetric coordinate-space. We expect the two-neutron deformed halos could be confirmed experimentally in the near future.

2. The Theoretical Framework

The Skyrme-HFB calculations are performed with the HFB-AX solver based on the B-spline method in a two-dimensional coordinate space [13]. Such an approach has been successfully used to describe the properties of weakly bound deformed nuclei around the neutron drip line. Generally, with a sufficiently large box and small mesh sizes, the description of the continuum spectrum would be very precise [14]. In present calculations, we adopt a coordinate-space of 21 fm and a maximum lattice mesh of 0.6 fm, respectively.

The HFB equation in the coordinate-space can be written as [13,21]:

$$\begin{bmatrix} h(r)-\lambda & \Delta(r) \\ \Delta^*(r) & h(r)-\lambda \end{bmatrix} \begin{bmatrix} U_k(r) \\ V_k(r) \end{bmatrix} = E_k \begin{bmatrix} U_k(r) \\ V_k(r) \end{bmatrix}, \tag{1}$$

where h is the single-particle Hamiltonian; λ is the Fermi surface energy or chemical potential; Δ is the pairing potential; U_k and V_k are the upper and lower components of quasi-particle wave functions; and E_k denotes the quasi-particle energy. For the particle-hole interaction channel, the SkM$^*_{\text{ext1}}$ and UNEDF0$_{\text{ext1}}$ [20] forces are adopted in $h(r)$, respectively. Note that SkM$^*_{\text{ext1}}$ and UNEDF0$_{\text{ext1}}$ forces include an additional higher-order density-dependent term as in Ref. [19]. In the particle-particle channel, a density-dependent pairing interaction is adopted as follows [22,23],

$$\Delta(r) = V_0 \left\{ 1 - \eta \left[\frac{\rho(r)}{\rho_0(r)} \right]^{\gamma} \right\}, \tag{2}$$

where $\rho_0(r)$ is the nuclear saturation density of 0.16 fm^3 and V_0, η, γ are three adjustable parameters. For different η, γ, there are four types of pairing interactions:

1. Volume pairing: $\eta = 0$;
2. Surface pairing: $\eta = 1, \gamma = 1$;
3. Mix pairing: $\eta = 0.5, \gamma = 1$;
4. New pairing: $\eta = 0.8, \gamma = 0.7$.

With a pairing window of 60 MeV, we adjusted pairing strength V_0 with the SkM$^*_{\text{ext1}}$ force to regularize the neutron pairing gap of ^{120}Sn to be $\Delta_n = 1.245$ MeV. The adjusted pairing strengths V_0 are 146.5 MeV, 467.5 MeV, 233.5 MeV, and 389.8 MeV corresponding to volume, surface, mix, and new pairing types, respectively. Note that results with different pairing interactions are more or less similar for stable nuclei. However, the pairing gaps could be very different towards drip lines by using different pairing interaction forms [23]. The surface pairing would lead to very large pairing gaps towards the neutron drip line, while volume pairing is on the contrary. The mixing pairing and new pairing are between the surface and volume pairings [23].

The particle density $\rho(r)$ and the pairing density $\tilde{\rho}(r)$ of even–even nuclei are expressed as,

$$\begin{aligned} \rho(r) &= 2\sum_k V_k^*(r)V_k(r), \\ \tilde{\rho}(r) &= -2\sum_k V_k(r)U_k^*(r), \end{aligned} \tag{3}$$

where in the sum, the quasiparticle energy cutoff is taken as $(60 - \lambda)$ MeV. To describe the odd-mass nuclei, the quasiparticle blocking is invoked. By blocking quasiparticles at the state μ, the density $\rho_B^\mu(r)$ and the pairing density $\tilde{\rho}_B^\mu(r)$ of odd-mass nuclei become [24],

$$\begin{aligned} \rho_B^\mu(r) &= U_\mu(r)U_\mu^*(r) + V_\mu^*(r)V_\mu(r) + 2\sum_{k\neq\mu} V_k^*(r)V_k(r), \\ \tilde{\rho}_B^\mu(r) &= -2\sum_{k\neq\mu} V_k(r)U_k^*(r). \end{aligned} \tag{4}$$

Besides, the particle number equation for the odd-mass nuclei has to be modified. The quasiparticle blocking is necessary for descriptions of ^{39}Na.

3. Results and Discussion

Figure 1 shows the two-neutron separation energies S_{2n} of sodium isotopes and magnesium isotopes based on the SkM$^*_{\text{ext1}}$ force and UNEDF0$_{\text{ext1}}$ force with the new pairing interaction. As expected, calculated S_{2n} decreases gradually towards the drip line. In both calculations, ^{39}Na is the drip line nucleus. In experiments, ^{39}Na is mostly likely to be the drip line since only one event was observed [8]. For magnesium isotopes, SkM$^*_{\text{ext1}}$ predicts ^{42}Mg as the drip-line nucleus, while UNEDF0$_{\text{ext1}}$ predicts ^{44}Mg as the drip line. UNEDF0$_{\text{ext1}}$ also predicts a slightly larger S_{2n} for ^{39}Na than SkM$^*_{\text{ext1}}$. In fact, the drip-line locations of Na and Mg isotopes are very different by using various mass models. In the macroscopic–microscopic model, the drip line locations are at ^{39}Na and ^{40}Mg [25]. The WS4 model predicts that ^{37}Na and ^{40}Mg are the drip line nuclei [26], which slightly underestimates the neutron drip lines. The Gogny-HFB calculations with the D1S force [27] predict that the drip lines are at ^{35}Na and ^{40}Mg. The HFB-21 calculations [28] predict ^{37}Na and ^{42}Mg. The Relativistic-Hartree–Bogoliubov [29] predict ^{45}Na and ^{46}Mg as the drip lines, which significantly overestimate the neutron drip lines. Thus, ^{39}Na as the drip line provides a stringent constraint on various theoretical models. With this constraint, we can more confidently infer that ^{42}Mg is also weakly bound. However, it is difficult to predict whether ^{44}Mg barely exists or not.

The halo properties of ^{39}Na and ^{42}Mg are dependent on the choices of Skyrme forces. We display the rms radii of neutron distributions in Na and Mg isotopes in Figure 2. As shown in Figure 2, the neutron radii by UNEDF0$_{\text{ext1}}$ force increase almost linearly with increasing neutron numbers. It can be seen that the neutron radii by SkM$^*_{\text{ext1}}$ are particularly enhanced for ^{39}Na. Note that UNEDF0$_{\text{ext1}}$ predicts larger S_{2n} than that by SkM$^*_{\text{ext1}}$. Thus the larger neutron radii by UNEDF0$_{\text{ext1}}$ are not due to weakly bound effects, but due to larger deformations.

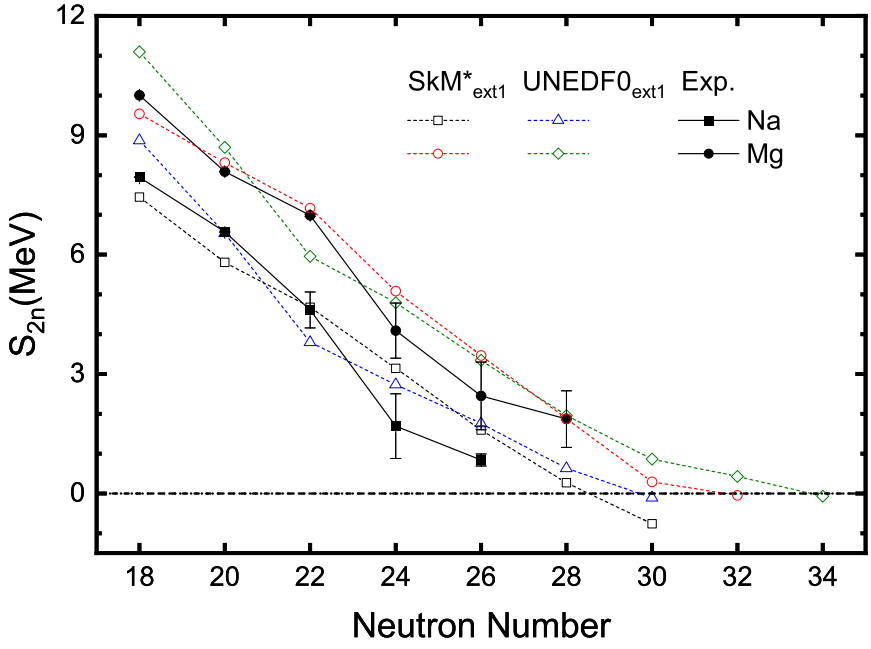

Figure 1. The two-neutron separation energies S_{2n} of Na and Mg isotopes obtained by the SkM^*_{ext1} force and $UNEDF0_{ext1}$ force with the new pairing interaction. Experimental data labeled by solid symbols are taken from Ref. [30].

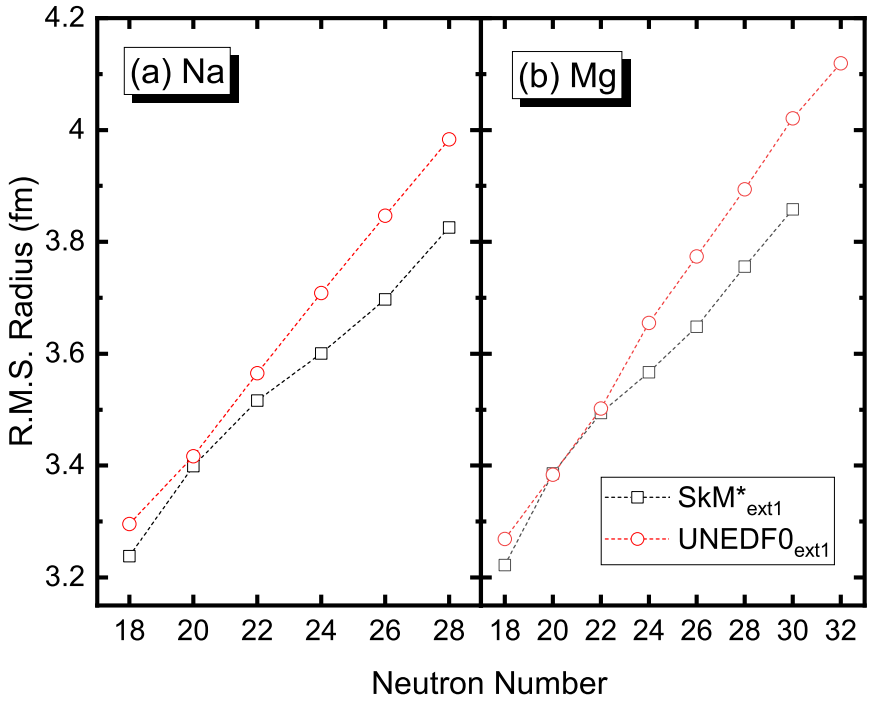

Figure 2. The calculated r.m.s. neutron radius in Na (**a**) and Mg (**b**) isotopes. Calculations are performed with SkM^*_{ext1} and $UNEDF0_{ext1}$ forces, respectively.

It is expected that the pairing is crucial for descriptions of weakly bound nuclei. Presently, four types of pairing interactions are used: volume, surface, mix, and new pairing interactions. For ^{39}Na, the neutron Fermi energy λ_n and two-neutron separation energies S_{2n} are -0.20 MeV (0.82 MeV), -0.48 MeV (0.67 MeV), -0.16 MeV (0.63 MeV), and -0.26 MeV (0.27 MeV), corresponding to volume, surface, mix, and new pairing interactions, respectively. Figure 3 displays the deformed halo structures of density distributions by different pairing interactions and the SkM^*_{ext1} force for ^{39}Na. The mixed pairing results

in the highest neutron Fermi surface energy λ_n, and it predicts the most significant halo structures. On the contrary, the surface pairing has a lowest λ_n, and it is less weakly bound with a less prominent halo structure. It is understandable that the surface pairing can bring more binding effects for weakly bound nuclei. The density distributions are shown in the cylindrical coordinates. The differences along z-axis and r-axis reflect the deformation effects in density distributions. We see that all the core density distributions have good prolate deformations. However, the surface halo shapes are very different. The surface pairing leads to the smallest surface deformations, while the volume pairing leads to the largest surface deformations. Hence, the surface halo deformations are very much dependent on the density dependencies of pairing interactions.

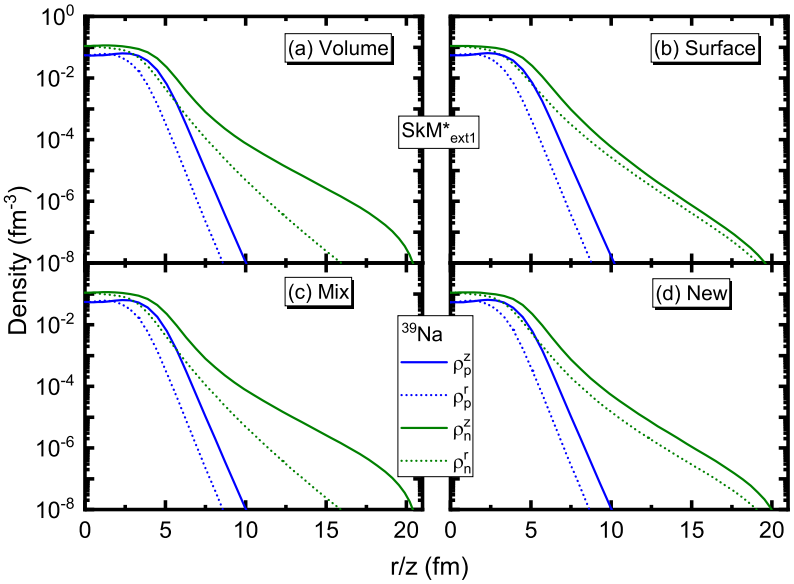

Figure 3. The density distributions of ^{39}Na obtained with various pairing interactions in the cylindrical coordinate spaces $\rho(r,z)$. Panel lists as (**a**) volume, (**b**) surface, (**c**) mix, and (**d**) new pairing interactions. The solid lines and dotted lines denote the density profiles along z-axis and r-axis.

Figure 4 shows the density distributions of ^{42}Mg by calculations with the SkM$^*_{\rm ext1}$ force and various pairing interactions. Note that ^{42}Mg is slightly unbound with volume and mixing pairing interactions. For ^{42}Mg, the neutron Fermi energy λ_n (and two-neutron separation energies S_{2n}) is -0.43 MeV (-0.20 MeV), -0.50 MeV (0.66 MeV), -0.37 MeV (-0.12 MeV), and -0.32 MeV (0.29 MeV), corresponding to volume, surface, mix, and new pairing interactions, respectively. It is consistent with ^{39}Na that the surface pairing results in more binding energies and could slightly extend the neutron drip line. The core densities all have good prolate deformations. However, the surface halos by surface pairing and new pairing are almost spherical. This is similar to the situation of ^{39}Na. The different deformation between the core and the halo in weakly bound nuclei is called shape decoupling effect. Exotic shape decoupling effects in deformed halo nuclei are of strong interest [31]. The pygmy dipole resonance is a possible probe of shape decoupling effects [23].

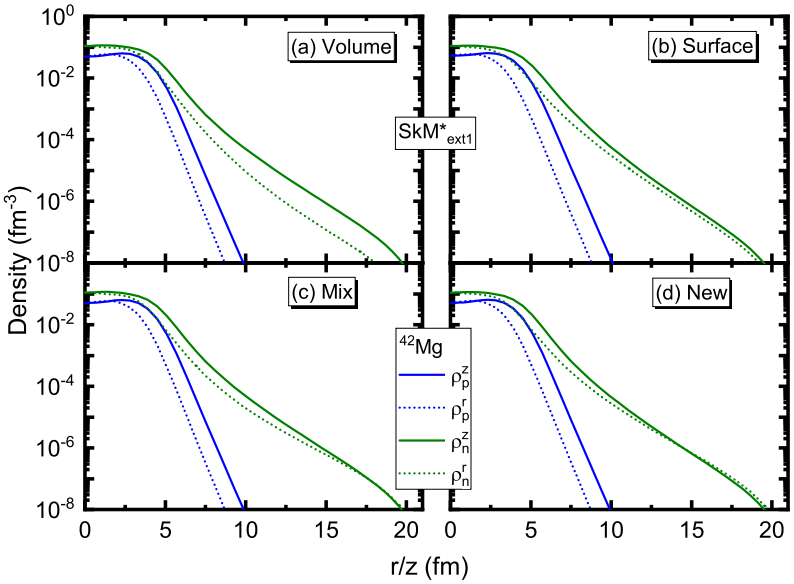

Figure 4. Similar to Figure 3, but for ^{42}Mg. Panel lists as (**a**) volume, (**b**) surface, (**c**) mix, and (**d**) new pairing interactions.

4. Conclusions

We have studied the deformed halo structures of drip-line nuclei ^{39}Na and ^{42}Mg, based on coordinate-space Skyrme-HFB calculations. The experimental discovery of ^{39}Na provides a stringent constraint on various theoretical models. With this constraint, we infer that ^{42}Mg is weakly bound. The problem is quite interesting because two-neutron deformed halos have still not been discovered yet. Both ^{39}Na and ^{42}Mg have a prolate deformed core, but their halo deformations could be different by adopting different pairing interactions. The surface pairing can bring more binding energies to weakly bound nuclei and tends to obtain spherical halos. The volume pairing results in significant deformed halos. In conclusion, the surface halo shapes are very much dependent on the density dependencies of pairing interactions.

Author Contributions: Conceptualization, J.P.; methodology, J.P.; software, J.P.; validation, J.P. and F.X.; formal analysis, Q.C.; investigation, Q.C.; resources, Q.C.; data curation, Q.C.; writing—original draft preparation, Q.C.; writing—review and editing, J.P.; visualization, H.C. and M.Z.; supervision, Q.C.; project administration, J.P.; funding acquisition, Q.C., J.P. and F.X. All authors have read and agreed to the published version of the manuscript.

Funding: This research was funded by the National Natural Science Foundation of China under Grants No. 12047504, 11975032, 11835001, and 11961141003, the China Postdoctoral Science Foundation under Grant No. 2020M670012, the National Key R&D Program of China (Contract No. 2018YFA0404403), and the Launching Fund of Henan University of Technology (31401409).

Institutional Review Board Statement: Not applicable.

Informed Consent Statement: Not applicable.

Data Availability Statement: Data is contained within the article. If you could not reproduce any figures, please contact chaiqz@haut.edu.cn.

Acknowledgments: The authors acknowledge the computations in the present calculations by using Tianhe-1A located in Tianjin.

Conflicts of Interest: The authors declare no conflict of interest.

References

1. Tanihata, I. Structure of neutron-rich nuclei studied by radioactive beams: Neutron halo and soft E1 excitation. *Nucl. Phys. A* **1991**, *522*, 275c–292c. [CrossRef]
2. Fukuda, M.; Ichihara, T.; Inabe, N.; Kubo, T.; Kumagai, H.; Nakagawa, T.; Yano, Y.; Tanihata, I.; Adachi, M.; Asahi, K.; et al. Neutron halo in ^{11}Be studied via reaction cross sections. *Phys. Lett. B* **1991**, *268*, 339–344. [CrossRef]
3. Meng, J.; Ring, P. Relativistic Hartree-Bogoliubov description of the neutron halo in ^{11}Li. *Phys. Rev. Lett.* **1996**, *77*, 3963–3966. [CrossRef] [PubMed]
4. Nakamura, T.; Kobayashi, N.; Kondo, Y.; Satou, Y.; Aoi, N.; Baba, H.; Deguchi, S.; Fukuda, N.; Gibelin, J.; Inabe, N.; et al. Halo structure of the island of inversion nucleus ^{31}Ne. *Phys. Rev. Lett.* **2009**, *103*, 262501. [CrossRef]
5. Kobayashi, N.; Nakamura, T.; Kondo, Y.; Tostevin, J.A.; Utsuno, Y.; Aoi, N.; Baba, H.; Barthelemy, R.; Famiano, M.A.; Fukuda, N.; et al. Observation of a *p*-wave one-neutron halo configuration in ^{37}Mg. *Phys. Rev. Lett.* **2014**, *112*, 242501. [CrossRef]
6. Jian, H.; Gao, Y.; Dai, F.; Liu, J.; Xu, X.; Yuan, C.; Kaneko, K.; Sun, Y.; Liang, P.; Shi, G.; et al. β-delayed γ emissions of ^{26}P and its mirror asymmetry. *Symmetry* **2021**, *13*, 2278. [CrossRef]
7. Tanihata, I.; Savajols, H.; Kanungo, R. Recent experimental progress in nuclear halo structure studies. *Prog. Part. Nucl. Phys.* **2013**, *68*, 215–313. [CrossRef]
8. Ahn, D.S.; Fukuda, N.; Geissel, H.; Inabe, N.; Iwasa, N.; Kubo, T.; Kusaka, K.; Morrissey, D.J.; Murai, D.; Nakamura, T.; et al. Location of the neutron dripline at fluorine and neon. *Phys. Rev. Lett.* **2019**, *123*, 212501. [CrossRef] [PubMed]
9. Baumann, T.; Amthor, A.M.; Bazin, D.; Brown, B.A.; Folden, C.M., III; Gade, A.; Ginter, T.N.; Hausmann, M.; Matoš, M.; Morrissey, D.J.; et al. Discovery of ^{40}Mg and ^{42}Al suggests neutron drip-line slant towards heavier isotopes. *Nature* **2007**, *449*, 1022–1024. [CrossRef]
10. Chai, Q.Z.; Pei, J.C.; Fei, N.; Guan, D.W. Constraints on the neutron drip line with the newly observed ^{39}Na. *Phys. Rev. C* **2020**, *102*, 014302. [CrossRef]
11. Terasaki, J.; Flocard, H.; Heenen, P.H.; Bonche, P. Deformation of nuclei close to the two-neutron drip line in the Mg region. *Nucl. Phys. A* **1997**, *621*, 706–718. [CrossRef]
12. Crawford, H.L.; Fallon, P.; Macchiavelli, A.O.; Doornenbal, P.; Aoi, N.; Browne, F.; Campbell, C.M.; Chen, S.; Clark, R.M.; Cortés, M.L.; et al. First spectroscopy of the near drip-line nucleus ^{40}Mg. *Phys. Rev. Lett.* **2019**, *122*, 052501. [CrossRef] [PubMed]
13. Pei, J.C.; Stoitsov,M.V.; Fann, G.I.; Nazarewicz, W.; Schunck, N.; Xu, F.R. Deformed coordinate-space Hartree-Fock-Bogoliubov approach to weakly bound nuclei and large deformations. *Phys. Rev. C* **2008**, *78*, 064306. [CrossRef]
14. Zhang, Y.N.; Pei, J.C.; Xu, F.R. Hartree-Fock-Bogoliubov descriptions of deformed weakly bound nuclei in large coordinate spaces. *Phys. Rev. C* **2013**, *88*, 054305. [CrossRef]
15. Skyrme, T. CVII. The nuclear surface. *Phil. Mag.* **1956**, *1*,1043–1054. [CrossRef]
16. Bartel, J.; Quentin, P.; Brack, M.; Guet, C.; Håkansson, H.B. Towards a better parametrisation of Skyrme-like effective forces: A critical study of the SkM force. *Nucl. Phys. A* **1982**, *386*, 79–100. [CrossRef]
17. Chabanat, E.; Bonche, P.; Haensel, P.; Meyer, J.; Schaeffer, R. A Skyrme parametrization from subnuclear to neutron star densities Part II. Nuclei far from stabilities. *Nucl. Phys. A* **1998**, *635*, 231–256. [CrossRef]
18. Kortelainen, M.; Lesinski, T.; Moré, J.; Nazarewicz, W.; Sarich, J.; Schunck, N.; Stoitsov, M.V.; Wild, S. Nuclear energy density optimization. *Phys. Rev. C* **2010**, *82*, 024313. [CrossRef]
19. Xiong, X.Y.; Pei, J.C.; Chen, W.J. Extension and parametrization of high-order density dependence in Skyrme forces. *Phys. Rev. C* **2016**, *93*, 024311. [CrossRef]
20. Zuo, Z.W.; Pei, J.C., Xiong, X.Y.; Zhu, Y. Global analysis of Skyrme forces with high-order density dependencies. *Chin. Phys. C* **2018**, *42*, 064106. [CrossRef]
21. Dobaczewski, J.; Flocard, H.; Treiner, J. Hartree-Fock-Bogoliubov description of nuclei near the neutron-drip line. *Nucl. Phys. A* **1984**, *422*, 103–139. [CrossRef]
22. Pastore, A.; Barranco, F.; Broglia, R.A.; Vigezzi, E. Microscopic calculation and local approximation of the spatial dependence of the pairing field with bare and induced interactions. *Phys. Rev. C* **2008**, *78*, 024315. [CrossRef]
23. Wang, K.; Kortelainen, M.; Pei, J.C. Probing surface quantum flows in deformed pygmy dipole modes. *Phys. Rev. C* **2017**, *96*, 031301(R). [CrossRef]
24. Bertsch, G.; Dobaczewski, J.; Nazarewicz, W.; Pei, J.C. Hartree-Fock-Bogoliubov theory of polarized Fermi systems. *Phys. Rev. A* **2009**, *79*, 043602. [CrossRef]
25. Möller, P.; Sierk, A.J.; Ichikawa, T.; Sagawa, H. Nuclear ground-state masses and deformations: FRDM(2012). *At. Data Nucl. Data Tables* **2016**, *109*, 1–204. [CrossRef]
26. Wang, N.; Liu, M.; Wu, X.Z.; Meng, J. Surface diffuseness correction in global mass formula. *Phys. Lett. B* **2014**, *734*, 215–219. [CrossRef]
27. Hilaire, S.; Girod, M. Large-scale mean-field calculations from proton to neutron drip lines using the D1S Gogny force. *Eur. Phys. J. A* **2007**, *33*, 237–241. [CrossRef]
28. Goriely, S.; Chamel, N.; Pearson, J.M. Further explorations of Skyrme-Hartree-Fock-Bogoliubov mass formulas. XII. Stiffness and stability of neutron-star matter. *Phys. Rev. C* **2010**, *82*, 035804. [CrossRef]

29. Xia, X.W.; Lim, Y.; Zhao, P.W.; Liang, H.Z.; Qu, X.Y.; Chen, Y.; Liu, H.; Zhang, L.F.; Zhang, S.Q.; Kim, Y.; et al. The limits of the nuclear landscape explored by the relativistic continuum Hartree CBogoliubov theory. *At. Data Nucl. Data Tables* **2018**, *121*, 1–215. [CrossRef]
30. Wang, M.; Audi, G.; Kondev, G.G.; Huang, W.J.; Naimi, S.; Xu, X. The AME2016 atomic mass evaluation (II). Tables, graphs and references. *Chin. Phys. C* **2017**, *41*, 030003. [CrossRef]
31. Zhou, S.G.; Meng, J.; Ring, P.; Zhao, E.G. Neutron halo in deformed nuclei. *Phys. Rev. C* **2010**, *82*, 011301. [CrossRef]